Journal of The Electrochemical Society, **155** (3) P13-P20 (2008)
0013-4651/2008/155(3)/P13/8/$23.00 © The Electrochemical Society

Mixed Conductivity and Stability of $CaFe_2O_{4-\delta}$

V. V. Kharton,[a,z] E. V. Tsipis,[a,b] V. A. Kolotygin,[a] M. Avdeev,[c] A. P. Viskup,[d] J. C. Waerenborgh,[b] and J. R. Frade[a]

[a]*Department of Ceramics and Glass Engineering, CICECO, University of Aveiro, 3810-193 Aveiro, Portugal*
[b]*Chemistry Department, ITN/CFMC-UL, P-2686-953 Sacavém, Portugal*
[c]*Bragg Institute, Australian Nuclear Science and Technology Organization, Menai, New South Wales 2234, Australia*
[d]*Institute of Physicochemical Problems, Belarus State University, 220050 Minsk, Belarus*

The total conductivity of $CaFe_2O_{4-\delta}$, studied in the oxygen partial pressure range from 10^{-17} to 0.5 atm at 1023–1223 K, is predominantly p-type electronic under oxidizing conditions. The oxygen ion transference numbers determined by the steady-state oxygen permeation and faradaic efficiency measurements vary in the range of 0.2 to 7.2×10^{-4} at 1123–1273 K, increasing with temperature. No evidence of any significant cationic contribution to the conductivity was found. The Mössbauer spectroscopy, thermogravimetry, and X-ray diffraction (XRD) showed that the orthorhombic lattice of calcium ferrite is essentially intolerant to the oxygen vacancy formation and to doping with lower-valence cations, such as Co and Ni. The oxygen nonstoichiometry (δ) is almost negligible, 0.0046–0.0059 at 973–1223 K and $p(O_2) = 10^{-5}$–0.21 atm, providing a substantial dimensional stability of $CaFe_2O_{4-\delta}$ ceramics. The average linear thermal expansion coefficients, calculated from the controlled-atmosphere dilatometry and high-temperature XRD data, are $(9.6–13.9) \times 10^{-6}$ K^{-1} in the oxygen pressure range from 10^{-8} to 0.21 atm at 873–1373 K. Decreasing $p(O_2)$ results in a modest lattice contraction and in the p-n transition indicated by the conductivity and Seebeck coefficient variations. The phase decomposition of $CaFe_2O_{4-\delta}$ occurs at oxygen chemical potentials between the low-$p(O_2)$ stability limit of $Ca_2Fe_2O_{5-\delta}$ brownmillerite and the hematite/magnetite boundary in binary Fe–O system.
 [DOI: 10.1149/1.2823458]

Manuscript submitted September 27, 2007; revised manuscript received November 1, 2007.
Available electronically January 3, 2008.

Oxide materials with mixed oxygen-ionic and electronic conductivity attract significant attention for high-temperature electrochemical applications, in particular, electrodes of solid oxide fuel cells (SOFCs) and dense ceramic membranes for oxygen separation and partial oxidation of light hydrocarbons.[1-5] The general requirements associated with these applications include a high oxygen permeability, thermodynamic stability in a wide range of temperature and oxygen partial pressure, moderate thermal and chemical expansion, and low reactivity with CO_2 and water vapor that may be present in air or in hydrocarbon conversion products. A promising combination of the transport properties and stability is known for perovskite-related ferrites derived from $(A,Ln)FeO_{3-\delta}$, where A and Ln correspond to the alkaline-earth and rare-earth metal cations, respectively.[4,5] However, these materials may suffer from hydration and carbonation, which result in the surface decomposition and blocking of oxygen exchange, especially under elevated pressures necessary for efficient use of the membrane reactors and SOFCs.[4,6-11] The stability in CO_2- and H_2O-containing atmospheres can be improved by reducing the chemical activity of alkaline-earth cations and/or by decreasing their radii in order to lower thermodynamic favorability for interaction with carbon dioxide and steam.[10,11] The latter strategy increases tendencies to ordering in the oxygen sublattice and to transition of ferrite perovskites into the brownmillerite-like polymorphs.[4,11] Nonetheless, brownmillerite-type $Ca_2Fe_2O_{5\pm\delta}$ still exhibits a substantial ionic conductivity, 2×10^{-3} S/cm at 1173 K, in combination with modest thermal expansion coefficients (TECs), $(11–13) \times 10^{-6}$ K^{-1}.[12]

Another phase in the ternary Ca–Fe–O system, stable in a wide temperature range, is $CaFe_2O_4$.[13] The orthorhombic crystal structure of this compound (space group *Pbnm*, no. 62) has two distinct iron sites; Ca^{2+} cations occupy pseudotriangular tunnels formed by the corner- and edge-shared FeO_6 octahedra.[13-16] In air, the total electrical conductivity of $CaFe_2O_4$ is predominantly electronic, at least above 723 K.[15,17] The ionic contribution to the conductivity at elevated temperatures is mainly provided by O^{2-} anion migration.[17] The atomistic computer simulations[17] showed that the Ca^{2+} cation transport might also be possible, but is hampered due to energetic factors, namely, unfavorable vacancy formation in the calcium sites. In fact, a significant cationic conduction was only achieved when calcium is replaced by small Li^+ cations, charge-compensated by Sn^{4+} doping in the iron sublattice.[16,18] Information available on the defect formation and electronic transport processes in $CaFe_2O_4$ is still scarce.

This work was centered on the analysis of the oxygen partial pressure dependencies of total conductivity, ion transference numbers, and Seebeck coefficient of $CaFe_2O_4$. Particular emphasis was also focused on the chemical expansion induced by minor oxygen-nonstoichiometry variations and on stability of $CaFe_2O_4$ at reduced oxygen pressures. In addition, phase equilibria in $(Ca,Sr)(Fe,M)_2O_{4\pm\delta}$ (M = Cr, Mn, Ni, Co) systems were assessed in order to evaluate the solubility of dopants, which might be used to alter defect concentrations and transport properties of $CaFe_2O_4$.

Experimental

Submicrometer powder of $CaFe_2O_4$ was prepared by glycine-nitrate process (GNP)[19] using $Ca(NO_3)_2 \cdot 4H_2O$ and $Fe(NO_3)_3 \cdot 9H_2O$ as starting materials. The molar glycine/nitrate ratio was double the stoichiometric value calculated, assuming that N_2, CO_2, and H_2O are the only gaseous reaction products. After synthesis, the powder was annealed at 1173 K for 2 h to remove organic residuals and pressed at 150–200 MPa. Gas-tight ceramic samples with relative density higher than 95% were sintered in air at 1423 K for 15 h and then slowly cooled (1–2 K/min) to achieve equilibrium oxygen content at low temperatures. The overall cation composition was confirmed by the inductively coupled plasma (ICP) spectroscopic analysis, which showed that the deviation from nominal Ca/Fe cation ratio is within the limits of experimental error (<0.1 atom %); the same conclusion was drawn earlier on the basis of Rietveld refinement results.[17] The powdered samples necessary for X-ray diffraction (XRD), Mössbauer spectroscopy, and thermogravimetric analysis (TGA) were obtained by grinding sintered ceramics. Additional series of ceramic samples used for the analysis of phase composition and iron states at elevated temperatures were annealed in various atmospheres for 20–25 h and then quenched.

The procedure to prepare $Ca_{0.5}Sr_{0.5}Fe_2O_4$ and $CaFe_{1.5}M_{0.5}O_4$ (M = Cr, Mn, Ni, Co) was similar to that for undoped calcium ferrite. These powders were additionally annealed in air at

[z] E-mail: kharton@ua.pt

1273–1463 K for 50 h with multiple intermediate grindings and XRD inspections; ceramic samples were sintered at 1423–1593 K.

Detailed descriptions of experimental techniques and equipment used for materials characterization can be found elsewhere.[6,7,11,12,20-23] The room-temperature XRD patterns were collected using a Rigaku D/MAX-B diffractometer (Cu Kα) radiation, 2θ = 10–100°, step 0.02°). The high-temperature XRD studies were conducted on a Philips X'Pert Pro instrument (2θ = 5–80°, step 0.015°, Anton Paar HTK-2000 heating stage) at 298–1373 K in air or under vacuum (total pressure of 5×10^{-8} to 5×10^{-7} atm); the equilibration time was 1–4 h. Rietveld analysis of the diffraction data was performed using the GSAS suite with EXPGUI frontend[24,25] and Fullprof software.[26] The microstructural studies were carried out using a Hitachi S-4100 scanning electron microscope (SEM) equipped with a Rontec ultrahigh vacuum detection system for energy-dispersive spectroscopy (EDS). The Mössbauer spectra were obtained at 295 K in transmission mode using a conventional constant-acceleration spectrometer and a 25 mCi ^{57}Co source in Rh matrix; the velocity scale was calibrated using α-Fe foil. The spectra were fitted to lorentzian lines using a nonlinear least-squares method,[27] constraining the relative areas and linewidths of both peaks in each quadrupole doublet to remain equal. The total oxygen content was determined by TGA (Setaram SetSys 16/18 instrument); the measurements were carried out in flowing dry air and Ar at 973–1223 K (50 K steps with 2–20 h dwells), followed by complete reduction into calcium oxide and metallic iron in a flow of dried 10% H_2–90% N_2 gas mixture at 1373–1423 K for 35 h. A vertical Linseis L75V/1250 dilatometer was used to study thermal and chemical expansion. The dilatometric measurements were performed at 923–1223 K in air and in a flowing Ar–O_2 gas mixture where the oxygen partial pressure, $p(O_2)$, was fixed at 6×10^{-4} atm; the temperature steps and equilibration time at each temperature were 50 K and 2–7 h, respectively. The total conductivity (four-probe dc) and Seebeck coefficient were measured in the oxygen partial pressure range from 0.4 down to 8×10^{-15} atm at 650–1280 K, as described elsewhere.[20] The oxygen ionic transport was studied at 1123–1273 K by the steady-state oxygen permeability (OP) and faradaic efficiency (FE) techniques.[21-23] For all OP and FE data presented in this work, the oxygen partial pressure (p_2) at the membrane feed side (OP) or cathode (FE) corresponds to 0.21 atm. In the case of FE measurements under nonzero oxygen pressure gradients, the results were corrected for steady-state oxygen permeation fluxes; for each $p(O_2)$ gradient, the permeation flux was determined independently prior to the FE tests.[21,23]

Results and Discussion

Structural and microstructural characterization.— XRD analysis showed that both GNP-synthesized powder and sintered ceramics of $CaFe_2O_4$ are single-phase (Fig. 1a). The crystal structure was identified as orthorhombic (space group *Pbnm*); the unit cell parameters (Table I) correspond well to the literature data.[14,15,18] Table I lists selected bond lengths calculated from the XRD data. One typical SEM image showing the microstructure of dense $CaFe_2O_4$ ceramics is presented in Fig. 2. The average grain size was 5–12 μm; no compositional inhomogeneities were detected by the EDS analysis within the limits of experimental uncertainty.

The high-temperature XRD studies demonstrated that $CaFe_2O_4$ phase is stable in the approximate temperature ranges of 300–1400 K in air and 300–1000 K at $p(O_2) = 10^{-8}$–10^{-7} atm under vacuum (Fig. 3). Heating up to 1370 K in vacuum leads to decomposition into a mixture of $Ca_2Fe_2O_5$ brownmillerite and Fe_3O_4. The limited phase stability of $CaFe_2O_4$ in moderately reducing atmospheres was further confirmed by the data on total conductivity and thermopower vs oxygen partial pressure, discussed below.

Figure 1b presents the room-temperature XRD patterns of $Ca_{0.5}Sr_{0.5}Fe_2O_4$ and $CaFe_{1.5}M_{0.5}O_4$ (M = Cr, Mn, Ni, Co), all equilibrated in air. The substitution of chromium for iron in $CaFe_{1-x}Cr_xO_4$ leads to solid solution formation, at least up to x = 0.5. Brownmillerite-type $Ca_2(Fe,M)_2O_5$ and Fe_3O_4 phases were observed to segregate on doping with 25 mol % cobalt or nickel. In the XRD pattern of $CaFe_{1.5}Mn_{0.5}O_4$, the reflections of $CaFe_2O_4$ phase coexist with very small impurity peaks, in agreement with data[14] on a relatively narrow compositional range, where $Ca(Fe,Mn)_2O_4$ solid solution is formed. In the case of $Ca_{0.5}Sr_{0.5}Fe_2O_4$, the substitution of Ca^{2+} by larger Sr^{2+} cations causes complete decomposition into the brownmillerite- and $SrFe_{12}O_{19}$-based phases. These results show that the number of dopants, which could be used to modify ionic and electronic transport in $CaFe_2O_4$, is very limited. In fact, only the solubility of chromium seems sufficient for this purpose. However, the oxygen ionic conduction in $CaFe_2O_4$ occurs, at least to a significant extent, via the vacancy migration mechanism;[17] chromium cations are expected to exhibit a donorlike behavior and, thus, to decrease the oxygen vacancy concentration. Consequently, major attention in this work was focused on undoped $CaFe_2O_4$ ceramics; selected properties of $CaFe_{1.5}Cr_{0.5}O_4$ were assessed for the sake of comparison. Note that the low solubility of acceptor-type dopants, such as $Ni^{2+/3+}$, suggests that the orthorhombic lattice of $CaFe_2O_4$ is almost intolerant to the oxygen vacancy formation.

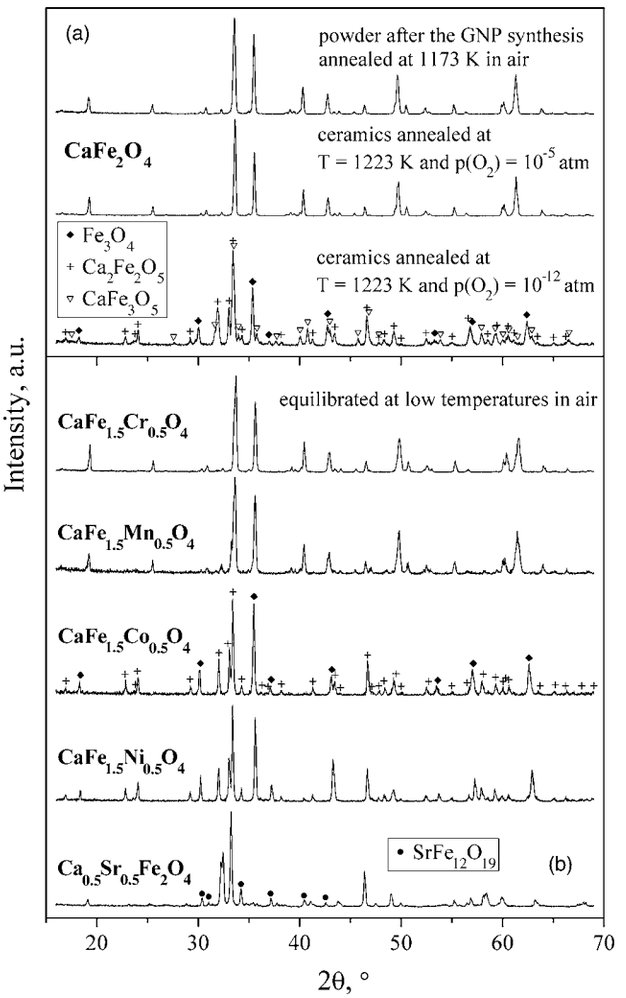

Figure 1. Room-temperature XRD patterns of undoped $CaFe_2O_4$ equilibrated in various atmospheres (a), and $CaFe_{1.5}M_{0.5}O_4$ (M = Cr, Mn, Co, Ni) and $Ca_{0.5}Sr_{0.5}Fe_2O_4$ samples equilibrated at atmospheric oxygen pressure (b). All unmarked reflections correspond to the parent orthorhombic phase.

Table I. Selected interatomic distances in $CaFe_2O_4$ lattice at room temperature.

Bond	Length, Å	Bond	Length, Å	Bond	Length, Å
Ca-O2×2	2.323(4)	Fe1-O3	2.031(6)	Fe2-O3×2	1.983(4)
Ca-O4×2	2.333(4)	Fe1-O4	2.045(5)	Fe2-O2×2	2.090(4)
Ca-O1×2	2.480(4)	Fe1-O1×2	2.052(3)	Fe2-O1	2.066(5)
Ca-O3	2.540(6)	Fe1-O1×2	2.098(3)	Fe2-O1	2.120(5)
Ca-O3	2.564(6)				

The unit cell parameters are a = 10.6969(2) Å, b = 9.2257(2) Å, and c = 3.0197(1) Å; space group *Pbnm* (no. 62); the agreement factors of structure refinement were R_p = 5.00%, R_{wp} = 6.68%, and χ^2 = 3.01.

Oxygen stoichiometry, Mössbauer spectra, and chemical expansion.— The thermogravimetric studies revealed that in oxidizing atmospheres, $CaFe_2O_{4-\delta}$ is almost oxygen stoichiometric, although a tendency to minor anion deficiency can be revealed. At 973–1223 K, the values of nonstoichiometry (δ) vary in the narrow ranges 0.0046–0.0048 in flowing dry air and 0.0056–0.0059 in argon, increasing on heating. These deviations from stoichiometry are larger than the reproducibility error, but the overall level of oxygen deficiency is very low, comparable to other possible experimental uncertainties. Such uncertainties might result, for example, from minor compositional inhomogeneities at the grain boundaries. At the same time, no essential deviations from the nominal cation composition were detected by the ICP and energy-dispersive spectroscopic analyses; moreover, these uncertainties cannot lead to the systematic variations of oxygen nonstoichiometry with the oxygen partial pressure, observed experimentally. Whatever the mechanism, the corresponding deviations of the average oxidation state of iron cations from 3+ are lower than the Mössbauer spectroscopy detection limits. Respectively, the room-temperature Mössbauer spectra of $CaFe_2O_{4-\delta}$ equilibrated under oxidizing or moderately reducing conditions consist of only two quadrupole doublets; for both signals, the isomer shift (IS) values are typical of octahedrally coordinated Fe^{3+} in the high-spin state[28,29] and the quadrupole splittings are similar to those reported in literature[30] (Fig. 4 and Table II). Neither Fe^{4+} nor Fe^{2+} cations can be detected, thus confirming that the oxygen deficiency is $<0.5\%$ in all cases. The estimated relative areas of the doublets, which relate to the two different crystallographic positions of iron in $CaFe_2O_{4-\delta}$ structure, are almost equal to each other

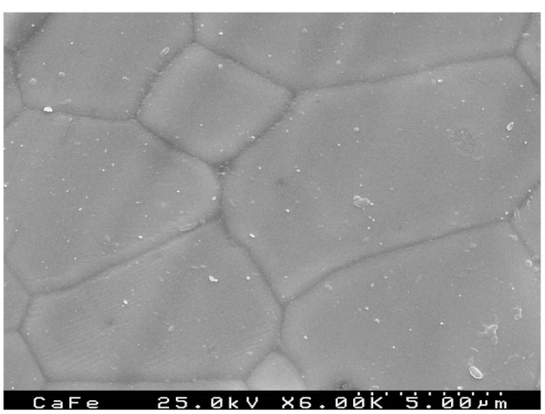

Figure 2. SEM images of polished and thermally etched $CaFe_2O_4$ ceramics.

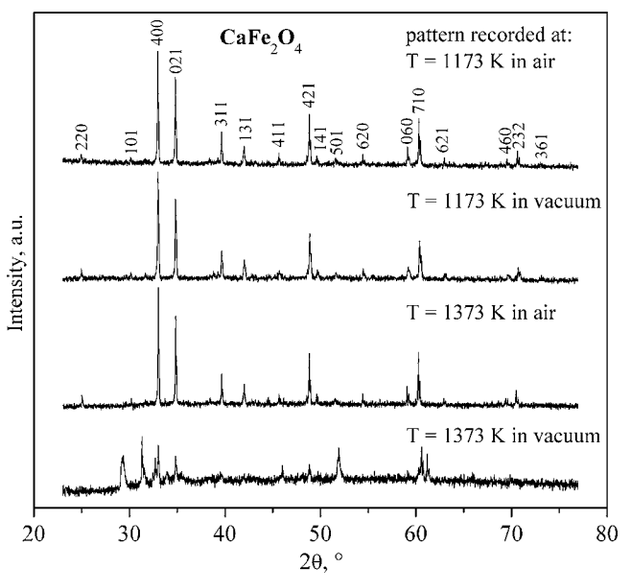

Figure 3. High-temperature XRD patterns of $CaFe_2O_{4-\delta}$ in air and in vacuum.

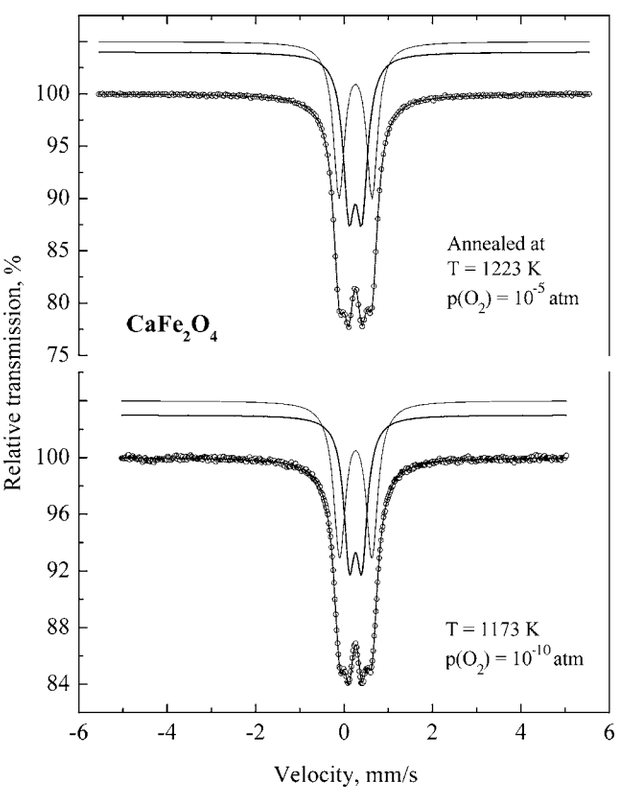

Figure 4. Room-temperature Mössbauer spectra of $CaFe_2O_{4-\delta}$ equilibrated at various oxygen partial pressures. The calculated functions plotted on the experimental data points are the sums of two quadrupole doublets (Table II), shown slightly shifted for clarity.

Table II. Parameters estimated from the room-temperature Mössbauer spectra of $CaFe_2O_{4-\delta}$.

Equilibration conditions	IS (mm/s)	QS (mm/s)	Γ (mm/s)	I (%)
Slowly cooled down to 295 K in air	0.37	0.30	0.32	49
	0.37	0.75	0.32	51
Annealed at 1223 K and $p(O_2) = 10^{-5}$ atm	0.37	0.29	0.31	49
	0.37	0.75	0.30	51
Annealed at 1173 K and $p(O_2) = 10^{-10}$ atm	0.37	0.28	0.30	44
	0.38	0.73	0.32	56

Notes: IS, QS, Γ, and I are the isomer shift relative to metallic α-Fe at 295 K, quadrupole splitting, full width at half maximum, and relative area, respectively. Estimated standard deviations are $<1\%$ for I and <0.02 mm/s for the other parameters.

for the samples equilibrated at low temperatures in air and annealed at 1223 K and $p(O_2) \approx 10^{-5}$ atm (Table II). Further reduction of the oxygen partial pressure down to 10^{-10} atm leads apparently to changing the iron site concentration ratio, probably due to local distortions and partial reorientation of FeO_6 polyhedra induced by oxygen losses. Similar behavior was observed earlier for acceptor-doped ferrite garnets, where the lattice packing is also not closest.[29] Note that $CaFe_2O_{4-\delta}$ remains single phase under these conditions.

The local structural changes near oxygen vacancies, in particular, tilting of the iron-oxygen octahedra, may also be responsible for the lattice contraction on reduction, which was revealed by both dilatometry (Fig. 5a) and high-temperature XRD (Fig. 6). One should mention that the average TECs calculated from the dilatometric and XRD data are in a good agreement, demonstrating reliability of the results. The TEC values determined by these two techniques at 873–1373 K in air are both equal to 13.9×10^{-6} K^{-1} (Table III). The lattice expansion on heating has an anisotropic character (Fig. 6), as for $Ca_2Fe_2O_5$ brownmillerite.[12] Because of the chemically induced lattice contraction on reduction, the average TECs decrease moderately with decreasing oxygen pressure. The incorporation of chromium cations in $Ca(Fe,Cr)_2O_4$ lowers the TECs (Fig. 5a and Table III) but raises chemical contraction (Fig. 5b). Regardless of these small changes, both $CaFe_2O_{4-\delta}$ and $CaFe_{1.5}Cr_{0.5}O_{4-\delta}$ ceramics appear to possess a relatively high dimensional stability on cycling the oxygen partial pressure and temperature as a result of low variations of the oxygen stoichiometry; their chemical expansivity is comparable to that of perovskite-type chromites[31] and layered nickelates.[32]

Electronic and ionic conduction.— The total conductivity (σ) of $CaFe_2O_{4-\delta}$ is lower than that of $Ca_2Fe_2O_{5-\delta}$ brownmillerite[12] (Fig. 7) but exhibits a similar activation energy (E_a), suggesting that electronic transport mechanisms in these phases are similar. Decreasing temperature leads to a progressive decrease of E_a values from 50 to 23 kJ/mol (Table IV), in correlation with the oxygen nonstoichiometry changes. The latter tendency seems to support the above hypothesis on significant lattice distortions near oxygen vacancies. Doping with chromium has a rather negligible effect on the conductivity at 870–1300 K and increases electronic transport in the low-temperature range.

The results on oxygen ionic conductivity (σ_O) calculated from the oxygen permeability and faradaic efficiency data (Fig. 8), confirm that the total conductivity of $CaFe_2O_{4-\delta}$ is predominantly electronic. The oxygen ion transference numbers vary in the range $(0.2–7.2) \times 10^{-4}$ at 1123–1273 K in air, increasing with temperature. Furthermore, as discussed below, the time-independent oxygen fluxes under either applied voltage (FE) or oxygen chemical potential gradients (OP) and the results of subsequent EDS analysis all

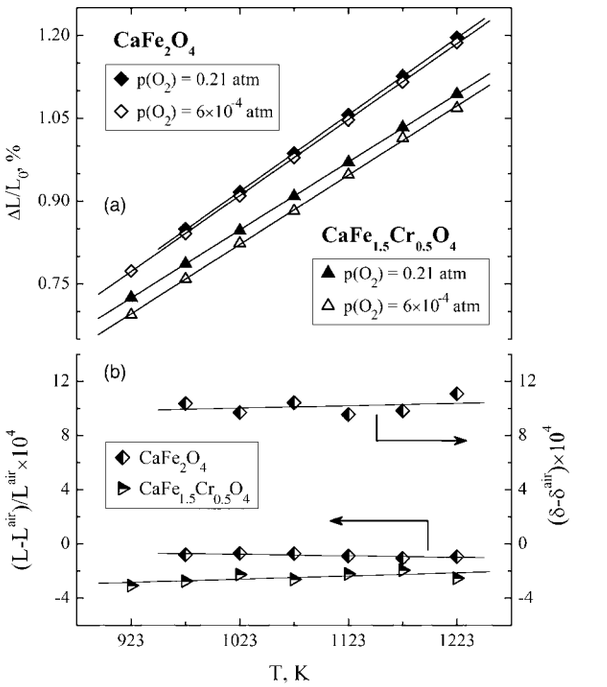

Figure 5. Dilatometric curves of $Ca(Fe,Cr)_2O_{4-\delta}$ ceramics at $p(O_2) = 0.21$ and 6×10^{-4} atm (a), and temperature dependence of the oxygen nonstoichiometry variations and relative length changes of $Ca(Fe,Cr)_2O_{4-\delta}$ ceramics on reducing oxygen partial pressure from 0.21 atm down to 1×10^{-5} and 6×10^{-4} atm, respectively (b). ΔL is the elongation with respect to the room-temperature length (L_0). L^{air} and δ^{air} are the length and oxygen deficiency at a given temperature in air, correspondingly. All data were collected on equilibration at each temperature during 2–20 h.

show that cationic conduction, if any, is much lower than oxygen anionic. This makes it possible to neglect the ionic contribution in the analysis of total conductivity and Seebeck coefficient (α) as function of the oxygen partial pressure.

Figure 9 shows the variations of electrical properties of $CaFe_2O_{4-\delta}$ in the $p(O_2)$ range, where no phase transformations were detected by XRD. In oxidizing atmospheres, the total conductivity and thermopower both decrease on reducing $p(O_2)$ under oxidizing conditions, whereas the Seebeck coefficient has a positive sign, unambiguously indicating the dominant role of the p-type electronic transport. At moderately lower oxygen pressures, a plateaulike behavior is observed. Further reduction leads to a conductivity minimum indicative of the p-n transition, which corresponds to approximately zero values of the Seebeck coefficient as marked by the dashed line in Fig. 9 for the isotherms at 1023 K. Beyond the minimum at still lower $p(O_2)$, the conductivity starts to increase due to the increasing contribution of n-type electronic transport; the Seebeck coefficient becomes negative.

Taking into account that the TGA and Mössbauer spectroscopy confirmed a predominantly trivalent state of iron cations in $CaFe_2O_{4-\delta}$, these trends may only be explained in terms of the electronic charge-carrier generation due to intrinsic disordering as a main factor governing the conductivity variations; the concentrations of mobile electrons and holes should be small compared to the corresponding densities of states. Another important conclusion refers to a relatively low mobility of the n-type charge carriers. The latter is directly evidenced by the fact that, in oxidizing and moderately reducing atmospheres when the hole concentration in oxygen-deficient $CaFe_2O_{4-\delta}$ should be lower than that of electrons according to the crystal electroneutrality condition, the p-type electronic conduction prevails. This phenomenon may originate from the strong energetic affinity of Fe^{2+} cations in $CaFe_2O_4$ to form binary

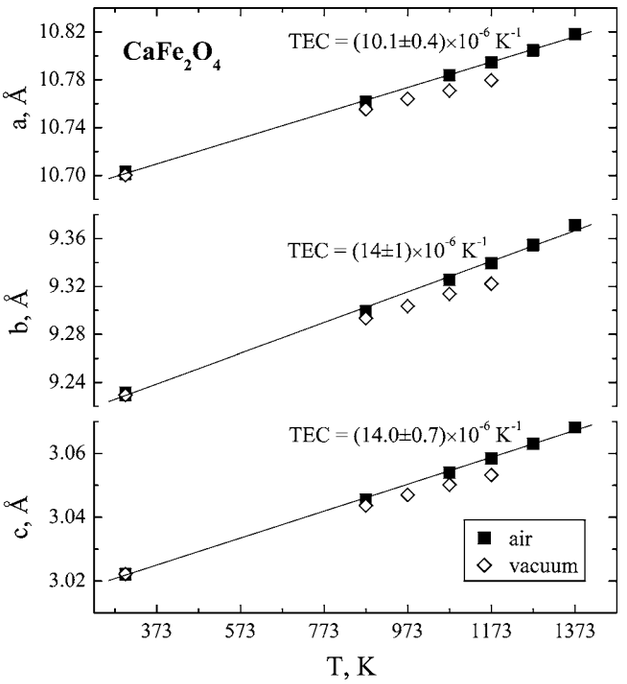

Figure 6. Temperature dependencies of the unit cell parameters of $CaFe_2O_{4-\delta}$ equilibrated in air and at the total pressure of 5×10^{-8} to 5×10^{-7} atm.

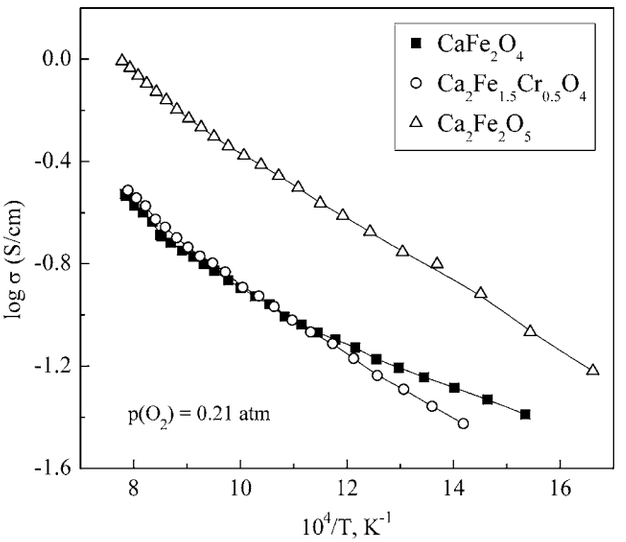

Figure 7. Temperature dependencies of the total conductivity of $CaFe_2O_{4-\delta}$ and $CaFe_{1.5}Cr_{0.5}O_{4-\delta}$ ceramics in air, compared to the data on brownmillerite-type $Ca_2Fe_2O_{5-\delta}$.[12]

and ternary clusters with oxygen vacancies as revealed by the computer simulations;[17] consequently, most of the n-type electronic charge carriers should be trapped. Whatever the trapping mechanisms, analogous behavior is well known for a variety of Fe-containing oxide phases with perovskite- and apatite-like structures (e.g., Ref. 33-35, and references cited).

Neglecting any site-exclusion effects and transported heat of the electronic charge carriers, the electrical conductivity, and Seebeck coefficient may be described as[33,36]

$$\sigma \approx (\mu_p \cdot p + \mu_n \cdot n) \cdot e \cdot N_{fu}/V_{uc} \quad [1]$$

$$\alpha \approx t_p \frac{k}{e} \ln\left(\frac{2}{p}\right) - (1 - t_p)\frac{k}{e} \ln\left(\frac{2}{n}\right) \quad [2]$$

where t_p is the hole transference number, n and p are the concentrations of electrons and holes per unit formula, μ_n and μ_p are their mobilities, $N_{fu} = 4$ is the number of formula units per unit cell, and V_{uc} is the unit-cell volume calculated from the XRD data. In these equations, all iron cations are assumed energetically equivalent because the Fe–O bond lengths for different crystallographic sites are quite similar (Table I). At the oxygen partial pressures close to atmospheric, high values of the Seebeck coefficient (Fig. 9b) suggest that $t_p \approx 1$. One can therefore estimate the hole concentration and mobility from the total conductivity and thermopower data by combining Eq. 1 and 2, neglecting the right side terms related to n-type electronic transport. The estimates of electron concentration can be obtained from the electroneutrality condition

$$2\delta + p = n \quad [3]$$

using the oxygen deficiency values determined by TGA. Increasing oxygen deficiency on reduction leads to the formation of n-type charge carriers, reflected by decreasing Seebeck coefficient. In these conditions, the values of μ_p, μ_n, p, n, and t_p can be derived using Eq. 1-3 in combination with the iron disproportionation constant

$$K_d = np \quad [4]$$

Typical results of such estimations are presented in Fig. 10a and b. As expected, the μ_p values are substantially higher than μ_n and decrease on reducing $p(O_2)$ due to raising local distortions induced by oxygen deficiency. The estimated hole mobility in air, 0.05–0.13 $cm^2\ V^{-1}\ s^{-1}$ at 1023–1223 K, is close to the characteristic threshold of 0.1 $cm^2\ V^{-1}\ s^{-1}$, considered to separate broadband and small-polaron conduction. This fact, and the decrease in μ_p values on heating, may argue in favor of the band mechanism. The estimated mobility of n-type charge carriers is lower than 8×10^{-4} $cm^2\ V^{-1}\ s^{-1}$ and is temperature-activated, indicative of polaron hopping. In addition, the apparent activation energy for the

Table III. Average linear thermal expansion coefficients of $Ca(Fe,Cr)_2O_{4-\delta}$ ceramics.

Composition	Method	T (K)	Atmosphere	TEC × 10^6 (K^{-1})
$CaFe_2O_4$	Dilatometry	973–1223	Air	13.9 ± 0.2
		923–1223	Ar–O_2[a]	13.8 ± 0.1
$CaFe_2O_4$	XRD	298–1373	Air	12.9 ± 0.8
		873–1373	Air	13.9 ± 1.2
		298–1173	Vacuum[b]	10.8 ± 0.7
		873–1173	Vacuum[b]	9.6 ± 0.7
$CaFe_{1.5}Cr_{0.5}O_4$	Dilatometry	923–1223	Air	12.31 ± 0.09
		923–1223	Ar–O_2[a]	12.5 ± 0.3

[a] $p(O_2) = 6 \times 10^{-4}$ atm.
[b] Total pressure in the range of 5×10^{-8} to 5×10^{-7} atm.

Table IV. Apparent activation energies for oxygen ionic and electronic transport in $CaFe_2O_{4-\delta}$.

Quantity (symbol)	T (K)	$p(O_2)$, atm	E_a (kJ/mol)
Total conductivity (σ)	653–923	0.21	23
	923–1173	0.21	34
	1193–1273	0.21	50
Oxygen ionic conductivity (σ_O)	1123–1273	0.21	325
n-type electronic conductivity σ_n	1023–1173	10^{-5}	129
Electron mobility (μ_n)	1023–1173	10^{-5}	122

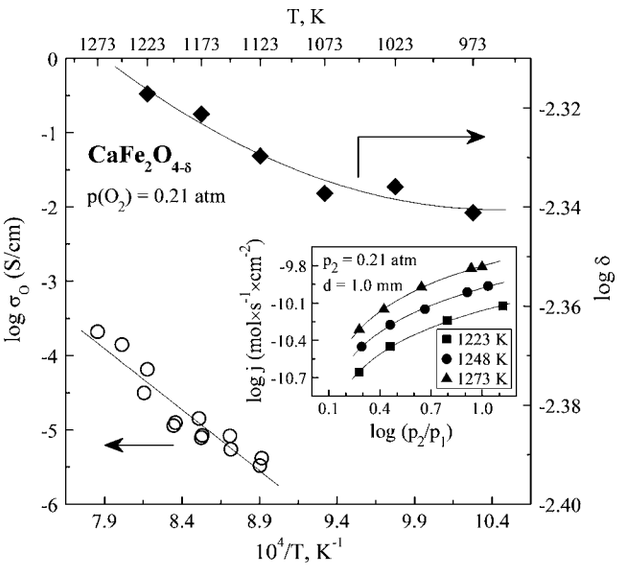

Figure 8. Temperature dependencies of the oxygen nonstoichiometry and oxygen ionic conductivity of $CaFe_2O_{4-\delta}$ ceramics in air. The ionic conductivity was calculated from the data on total conductivity and oxygen ion transference numbers determined by the oxygen permeability and faradaic efficiency measurements. The inset shows one example of the OP data for 1.0 mm thick membrane.

electron mobility (Table IV) is significantly higher than expected for a small-polaron mechanism, thus confirming the conclusion[17] on the formation of stable defect clusters involving Fe^{2+} cations and oxygen vacancies.

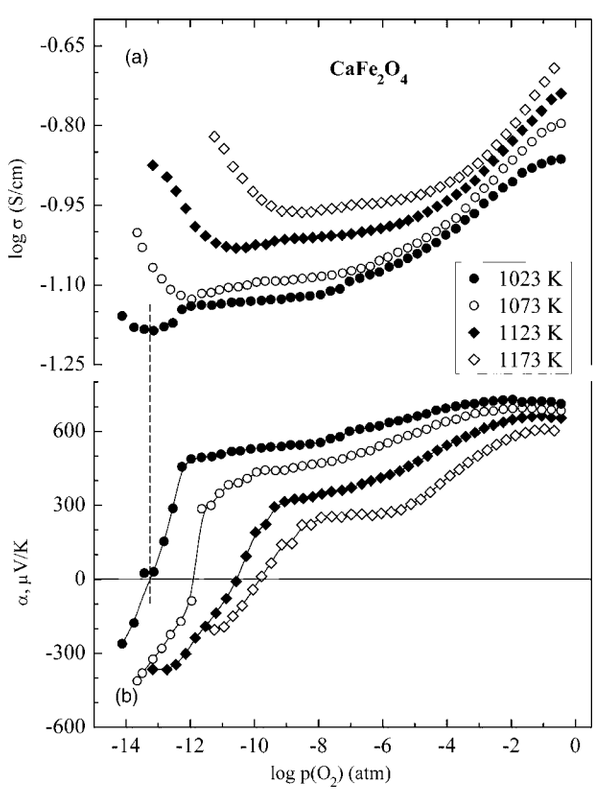

Figure 9. Oxygen partial pressure dependencies of the total conductivity (a) and Seebeck coefficient (b) of $CaFe_2O_{4-\delta}$.

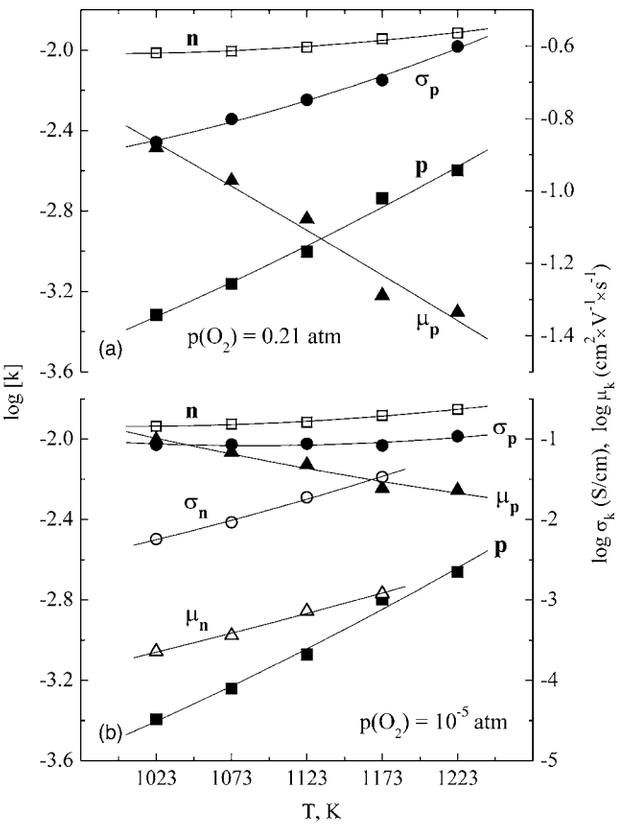

Figure 10. Temperature dependencies of the electronic charge carrier concentrations ([k]), mobilities (μ_k), and partial conductivities (σ_k) in air and at $p(O_2) = 10^{-5}$ atm, estimated from the total conductivity, Seebeck coefficient, and oxygen nonstoichiometry data (see text).

The latter conclusion is also validated by the weak dependence of oxygen transference numbers (t_O) on the oxygen partial pressure (Fig. 11), which results mainly from the variations of p-type electronic transport (Fig. 9). Such behavior indicates that the oxygen ionic conduction is essentially $p(O_2)$ independent due to a low concentration of mobile vacancies, determined by the cluster dissociation processes. In combination with structural constraints, this factor is responsible for very low ionic conductivity of $CaFe_2O_{4-\delta}$ (Fig. 8), whereas the activation energy (Table IV) is almost twice as high as the average oxygen-vacancy migration energy evaluated by the computer simulation studies, ~170 kJ/mol.[17] The oxygen fluxes through dense $CaFe_2O_{4-\delta}$ membranes placed under electrical and/or oxygen chemical potential gradients were time independent within the limits of experimental uncertainty; one typical example of the faradaic efficiency data is shown in the inset of Fig. 11. If calcium cationic transport would be significant, the oxygen fluxes should decrease with time owing to blocking of the electrodes (FE) or membrane surface (OP). Also, no traces of cation demixing caused by Ca^{2+} conduction were revealed by the EDS analysis of $CaFe_2O_{4-\delta}$ ceramics tested under applied voltage and $p(O_2)$ gradients during 300–1200 h, as illustrated by Fig. 12.

Behavior in reducing atmospheres.— Reducing $p(O_2)$ below 10^{-11}–10^{-16} atm at 1023–1223 K leads to a drastic increase of the total conductivity and Seebeck coefficient, followed by hysteresis phenomena on subsequent reoxidation (Fig. 13). Note that for the data on electrical properties in the vicinity of these hystereses, the equilibration times were as long as 25–60 h. The observed behavior is caused by $CaFe_2O_{4-\delta}$ phase decomposition into $Ca_2Fe_2O_{5-\delta}$ and Fe_3O_4 on reduction, in agreement with XRD analysis (Fig. 1a). The

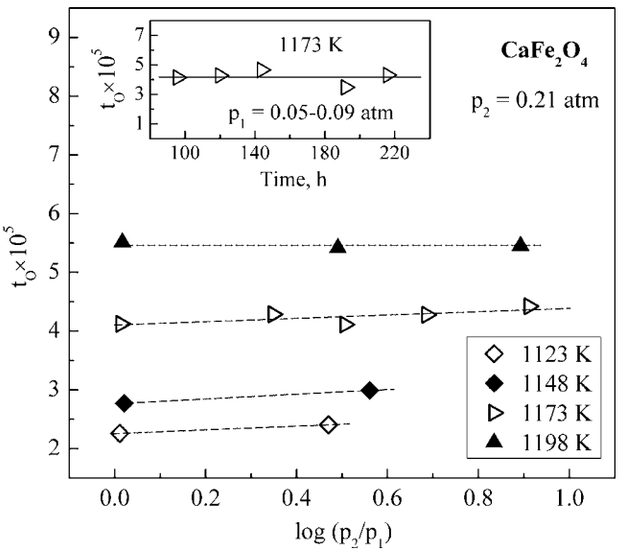

Figure 11. Oxygen-ion transference numbers of $CaFe_2O_{4-\delta}$, determined by the faradaic efficiency technique, as function of the oxygen pressure gradient. Inset shows one representative example of the time dependence of faradaic efficiency at 1173 K.

traces of $CaFe_3O_5$ phase visible in the XRD patterns of reduced $CaFe_2O_{4-\delta}$ appear due to kinetic reasons, namely, slow equilibration processes associated with a stagnated cation diffusion; the same reason is responsible for the conductivity hysteresis on reoxidation (Fig. 13).

At 1223 K, the decomposition of $CaFe_2O_{4-\delta}$ occurs at oxygen chemical potentials close to the hematite ↔ magnetite boundary in the binary Fe–O system[37] (Fig. 14), suggesting that this transition is induced by excessive lattice stress when the concentration of relatively large Fe^{2+} cations increases. Most likely, a similar nature associated with $CaFe_2O_{4-\delta}$ lattice relaxation near the point defects is relevant for the tendencies to local structural distortions and defect clustering on reduction. Whatever the microscopic mechanisms, the redox stability of $CaFe_2O_{4-\delta}$ appears considerably lower with respect to perovskite-like ferrites, where the average oxidation state of iron may vary in a wide range without structural collapse and the reductive decomposition is accompanied with metallic Fe

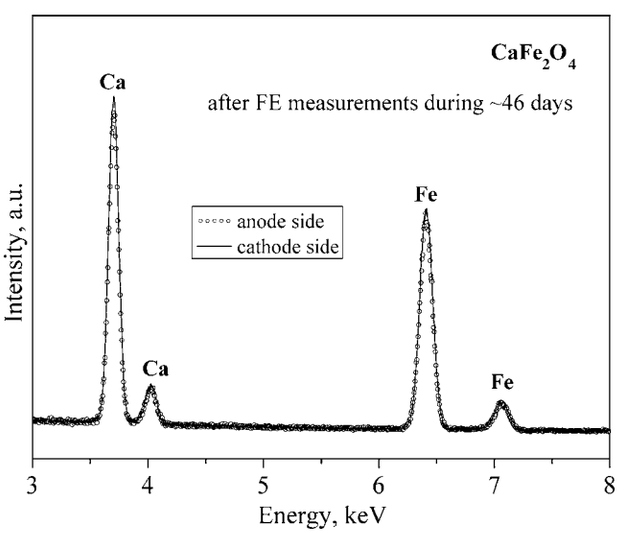

Figure 12. Comparison of the EDS spectra collected at the anode and cathode sides of $CaFe_2O_{4-\delta}$ ceramics after the faradaic efficiency tests under zero $p(O_2)$ gradient during more than 1100 h.

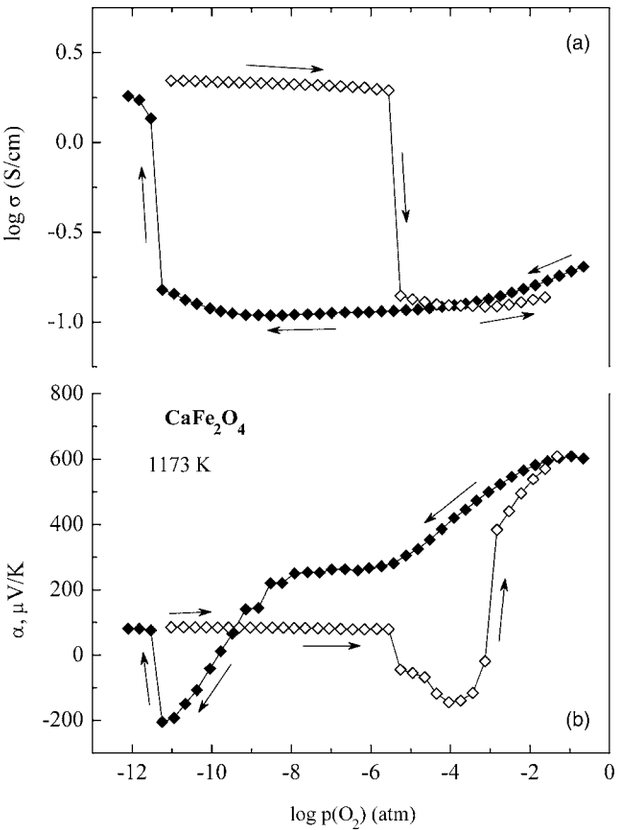

Figure 13. Example illustrating the variations of total conductivity (a) and Seebeck coefficient (b) of $CaFe_2O_{4-\delta}$ ceramics on reductive decomposition and subsequent reoxidation at 1173 K. Arrows show the direction of $p(O_2)$ changes.

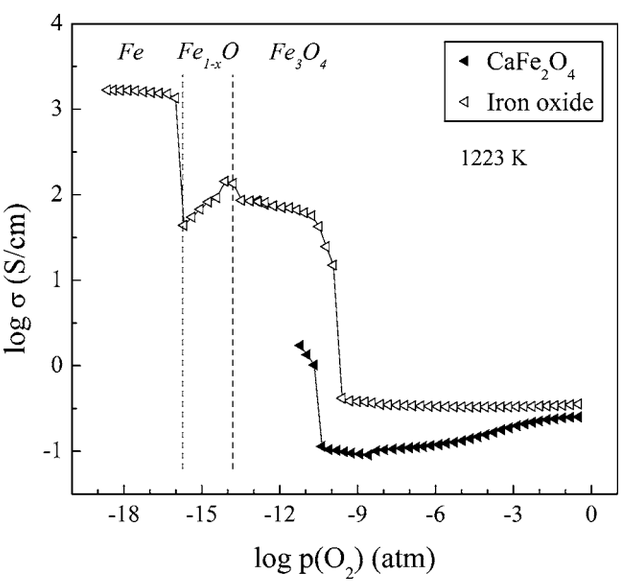

Figure 14. Oxygen partial pressure dependencies of the total conductivity of $CaFe_2O_{4-\delta}$ on reduction at 1223 K, compared to the data on binary iron oxide ceramics.

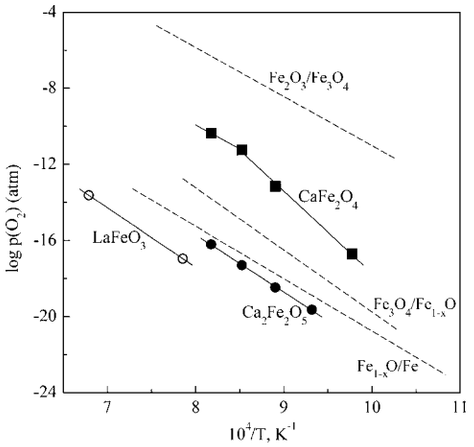

Figure 15. Low-$p(O_2)$ stability limits of $CaFe_2O_{4-\delta}$ compared to the data on $Ca_2Fe_2O_{5-\delta}$ brownmillerite,[12] perovskite-type $LaFeO_{3-\delta}$,[38] and binary iron oxides.[37]

segregation.[6,33,34,38] Figure 15 compares the approximate low-$p(O_2)$ stability limits of $CaFe_2O_{4-\delta}$, estimated from the oxygen partial pressure dependencies of electrical properties, and literature data on $LaFeO_{3-\delta}$,[38] $Ca_2Fe_2O_{5-\delta}$,[12] and binary iron oxides.[37]

Conclusions

Single-phase $CaFe_2O_{4-\delta}$ ceramics with density of >95% was prepared using the glycine-nitrate process and characterized by XRD, SEM/EDS, TGA, Mössbauer spectroscopy, controlled-atmosphere dilatometry, and measurements of the total conductivity, Seebeck coefficient, oxygen permeability, and faradaic efficiency. The thermogravimetric and Mössbauer spectroscopy studies showed that, in the oxygen partial pressure range where $CaFe_2O_{4-\delta}$ phase exists, the predominant oxidation state of iron cations is 3+. The oxygen deficiency of $CaFe_2O_{4-\delta}$ is as low as 0.0046–0.0059 at 973–1223 K and $p(O_2) = 10^{-5}$–0.21 atm. In combination with structural constraints and strong tendency to the formation of stable defect clusters involving oxygen vacancies and Fe^{2+} cations, revealed by static lattice simulations,[17] this factor leads to low oxygen-ionic and n-type electronic transport. At oxygen pressures close to atmospheric, the conductivity of $CaFe_2O_{4-\delta}$ is governed by the p-type electronic charge carriers formed due to iron disproportionation. The oxygen ion transference numbers determined by the oxygen permeation and faradaic efficiency techniques vary in the range $(0.2–7.2) \times 10^{-4}$ at 1123–1273 K in air. No evidence of any significant cationic contribution to the total conductivity was found. Decreasing oxygen chemical potential results in a modest contraction of orthorhombic $CaFe_2O_{4-\delta}$ lattice and in the transition to dominating n-type electronic conduction, followed by decomposition. The approximate phase stability limits estimated by the electrical measurements lie between those of $Ca_2Fe_2O_{5-\delta}$ brownmillerite and the hematite/magnetite boundary in binary Fe–O system. The average thermal expansion coefficients of $CaFe_2O_{4-\delta}$ ceramics, calculated from the dilatometric and high-temperature XRD data, are 9.6 to 13.9 $\times 10^{-6}$ K^{-1} in the oxygen partial pressure range from 10^{-8} to 0.21 atm at 873–1373 K. Although the dimensional stability of $CaFe_2O_{4-\delta}$ on reducing $p(O_2)$ might be of significant interest, the applicability of this compound for high-temperature electrochemical devices is very limited due to poor transport properties. The structure of $CaFe_2O_{4-\delta}$ comprising edge-shared FeO_6 octahedra may not tolerate extensive acceptor-type doping, increasing oxygen deficiency, and incorporation of larger cations in the calcium sites. In particular, the solubility of lower-valence cations, such as Co and Ni, is considerably lower than 25% of the iron site concentration. Doping with 25 mol % chromium leads to a moderately lower thermal expansion and higher chemically induced contraction and has a negligible effect on the total conductivity at elevated temperatures.

Acknowledgments

This work was supported by the Fundação para a Ciência e a Tecnologia (FCT), Portugal (projects no. POCI/CTM/58570/2004, PTDC/CTM/64357/2006, SFRH/BPD/28629/2006, and REEQ/710/CTM/2005). The experimental assistance of Y. Pivak and A. Yaremchenko is gratefully acknowledged.

University of Aveiro assisted in meeting the publication costs of this article.

References

1. B. C. H. Steele, *J. Mater. Sci.*, **36**, 1053 (2001).
2. J. A. Kilner, *Faraday Discuss.*, **134**, 9 (2007).
3. P. Singh and N. Q. Minh, *Int. J. Appl. Ceram. Technol.*, **1**, 5 (2004).
4. H. J. M. Bouwmeester and A. J. Burggraaf, in *Fundamentals of Inorganic Membrane Science and Technology*, A. J. Burggraaf and L. Cot, Editors, p. 435, Elsevier, Amsterdam (1996).
5. Y. Liu, X. Tan, and K. Li, *Catal. Rev. - Sci. Eng.*, **48**, 145 (2006).
6. V. V. Kharton, A. A. Yaremchenko, A. L. Shaula, A. P. Viskup, F. M. B. Marques, J. R. Frade, E. N. Naumovich, J. R. Casanova, and I. P. Marozau, *Defect Diffus. Forum*, **226–228**, 141 (2004).
7. V. V. Kharton, A. A. Yaremchenko, A. V. Kovalevsky, A. P. Viskup, E. N. Naumovich, and P. F. Kerko, *J. Membr. Sci.*, **163**, 307 (1999).
8. A. Kleinert, A. Feldhoff, T. Schiestel, and J. Caro, *Catal. Today*, **118**, 44 (2006).
9. H. Lu, J. Tong, Y. Cong, and W. Yang, *Catal. Today*, **104**, 154 (2005).
10. H. Yokokawa, N. Sakai, T. Kawada, and M. Dokiya, *Solid State Ionics*, **52**, 43 (1992).
11. V. V. Kharton, F. M. Figueiredo, A. V. Kovalevsky, A. P. Viskup, E. N. Naumovich, J. R. Jurado, and J. R. Frade, *Defect Diffus. Forum*, **186–187**, 119 (2000).
12. A. L. Shaula, Y. V. Pivak, J. C. Waerenborgh, P. Gaczyński, A. A. Yaremchenko, and V. V. Kharton, *Solid State Ionics*, **177**, 2923 (2006).
13. B. Philips and A. Muan, *J. Am. Ceram. Soc.*, **41**, 445 (1958).
14. S. Zouari, L. Ranno, A. Cheikh-Rouhou, M. Pernet, and P. Strobel, *J. Mater. Chem.*, **13**, 951 (2003).
15. F. Archaimbault, P. Odier, and J. Choisnet, *Solid State Ionics*, **28–30**, 1357 (1988).
16. L. F. Nazar, G. Goward, F. Leroux, M. Duncan, H. Huang, T. Kerr, and J. Gaubicher, *Int. J. Inorg. Mater.*, **3**, 191 (2001).
17. E. V. Tsipis, Y. V. Pivak, J. C. Waerenborgh, V. A. Kolotygin, A. P. Viskup, and V. V. Kharton, *Solid State Ionics*, **178**, 1428 (2007).
18. N. Sharma, K. M. Shaju, G. V. Subba Rao, and B. V. R. Chowdari, *J. Power Sources*, **124**, 204 (2003).
19. M. W. Murphy, T. R. Armstrong, and P. A. Smith, *J. Am. Ceram. Soc.*, **80**, 165 (1997).
20. M. V. Patrakeev, E. B. Mitberg, A. A. Lakhtin, I. A. Leonidov, V. L. Kozhevnikov, V. V. Kharton, M. Avdeev, and F. M. B. Marques, *J. Solid State Chem.*, **167**, 203 (2002).
21. V. V. Kharton, A. P. Viskup, A. V. Kovalevsky, F. M. Figueiredo, J. R. Jurado, A. A. Yaremchenko, E. N. Naumovich, and J. R. Frade, *J. Mater. Chem.*, **10**, 1161 (2000).
22. V. V. Kharton, A. L. Shaula, E. N. Naumovich, N. P. Vyshatko, I. P. Marozau, A. P. Viskup, and F. M. B. Marques, *J. Electrochem. Soc.*, **150**, J33 (2003).
23. V. V. Kharton, E. V. Tsipis, A. A. Yaremchenko, N. P. Vyshatko, A. L. Shaula, E. N. Naumovich, and J. R. Frade, *J. Solid State Electrochem.*, **7**, 468 (2003).
24. B. H. Toby, *J. Appl. Crystallogr.*, **34**, 210 (2001).
25. A. C. Larson and R. B. Von Dreele, Los Alamos National Laboratory report no. LAUR 86-748 (2004).
26. J. Rodríguez-Carvajal, *Physica B*, **192**, 55 (1993).
27. J. C. Waerenborgh, M. O. Figueiredo, J. M. P. Cabral, and L. C. J. Pereira, *J. Solid State Chem.*, **111**, 300 (1994).
28. C. A. McCammon, A. I. Becerro, F. Langenhorst, R. J. Angel, S. Marion, and F. Seifert, *J. Phys.: Condens. Matter*, **12**, 2969 (2000).
29. J. C. Waerenborgh, D. P. Rojas, A. L. Shaula, V. V. Kharton, and F. M. B. Marques, *Mater. Lett.*, **58**, 3432 (2004).
30. A. Hudson and H. J. Whitfield, *J. Chem. Soc. A*, 376 (1967).
31. A. Atkinson and T. M. G. M. Ramos, *Solid State Ionics*, **129**, 259 (2000).
32. V. V. Kharton, A. V. Kovalevsky, M. Avdeev, E. V. Tsipis, M. V. Patrakeev, A. A. Yaremchenko, E. N. Naumovich, and J. R. Frade, *Chem. Mater.*, **19**, 2027 (2007).
33. J. Mizusaki, *Solid State Ionics*, **52**, 79 (1992).
34. E. N. Naumovich, M. V. Patrakeev, V. V. Kharton, M. S. Islam, A. A. Yaremchenko, J. R. Frade, and F. M. B. Marques, *Solid State Ionics*, **177**, 457 (2006).
35. A. L. Shaula, V. V. Kharton, J. C. Waerenborgh, D. P. Rojas, and F. M. B. Marques, *J. Eur. Ceram. Soc.*, **25**, 2583 (2005).
36. P. Kofstad, *Nonstoichiometry, Diffusion and Electrical Conductivity in Binary Metal Oxides*, Wiley, New York (1972).
37. G. G. Charette and S. N. Flengas, *J. Electrochem. Soc.*, **115**, 796 (1968).
38. T. Nakamura, G. Petzow, and L. J. Gauckler, *Mater. Res. Bull.*, **14**, 649 (1979).